



Three-Dimensional Accurate Geometric Modeling and Mechanical Analysis of Wire Mesh for Deployable Antennas

Zhuolin Li* and Han Zhang†

Xidian University, 710071 Xi'an, People's Republic of China

Yusheng Li,‡ Xiaofei Wu,§ Zhilong Tan,¶ and Qingyan Qin**

Sino-Platinum Metals Co., Ltd., 650000 Kunming, People's Republic of China

and

Yiqun Zhang††

Xidian University, 710071 Xi'an, People's Republic of China

<https://doi.org/10.2514/1.J063784>

Wire meshes are widely used in deployable antennas, and the structure of the wire mesh directly affects the structural and electrical properties of the antenna. This study proposes a set of automated geometric modeling and mechanical analysis processes to realize the automated mechanical analysis and design of complex wire mesh structures. First, considering the tilt in the wire mesh structure owing to the traction of the underlap on the loop, a three-dimensional (3D) geometric model of the repeating unit of the wire mesh structure was established using periodic cubic spline curves. Subsequently, a method using sensitivity matrix adjustment is proposed to eliminate the interstructure inlay phenomenon, and an optimization model is established. The vector superposition method established a 3D geometric model of the overall wire mesh structure without an inlay problem. Finally, a finite element model of the wire mesh considering the contact problem was established by the adaptive matching method for contact pairs of the finite element model of the wire mesh. Mechanical simulation experiments were carried out on the model, comparing the theoretical analysis with the experimental results and verifying its reasonableness.

I. Introduction

SATELLITE antennas are widely used in many fields, such as space communication, electronic reconnaissance, navigation, remote sensing, and deep space exploration. With the improvement of the requirements of space missions, the demand for larger-aperture and higher-precision satellite antennas is more urgent. Deployable mesh reflector antennas, one of the most widely used satellite antennas in orbit, are characterized by a low surface density and simple structure [1,2]. A hoop truss antenna (a), a radial ribbed antenna (b), a deployable truss antenna (c), and a wrapped-rib antenna (d) are shown in Fig. 1.

One of the important features of the deployable mesh reflector antennas is that their reflective surface consists of a flexible wire mesh, which is laid on the front net to reflect electromagnetic waves, as shown in Fig. 2. To adapt to the folding and unfolding requirements, the mesh is made of extremely fine and soft metal wires based on the textile weaving process, and its structural form and weaving process are very complex. The purpose is, on the one hand, to make the mesh have a low coefficient of thermal expansion and enough structural rigidity to withstand large pretensions and resist the influence of the extreme environment in space, and, on the other hand, to ensure that the mesh structure has excellent isotropic properties to

facilitate the design and development of the overall structure of the antenna.

Wire mesh has various formations: it may be plain wave, weft-knitted, or warp-knitted. The warp-knitted wire mesh is widely used in antennas. The development of warp-knitted wire mesh is first knitted by a weaving machine for weaving production; the mechanical properties of the wire mesh are tested, and the weaving process is adjusted according to the test results [3]. The research method (production, testing, and adjustment) has the disadvantages of a long development cycle and high production costs. When the test results do not meet the demand, how to optimize the process lacks direction and chapter; therefore, it is necessary to carry out research from the perspective of theoretical analysis and design optimization.

To improve the above research method, we must establish an accurate three-dimensional (3D) geometric and finite element model of the warp-knitted wire mesh. Goktep [4,5,6] measured the geometrical parameters of warp-knitted fabrics, generalized the typical structure of the loop, obtained the parameterized control points describing the warp-knitted loop, and built a 3D geometrical model of the fabric using nonuniform rational B-spline curves and surfaces. Based on the Goktepe model, Cong et al. [7,8] realized a smooth connection between the loops by adding one control point near the first and last control points, and finally realized the 3D geometric modeling of warp-knitted loops. Xu et al. [9,10] defined the control points of the warp-knitted loop using 17 points and used the software TexGen to establish a 3D geometric model of a tricot stitch. However, these scholars neglected the inlay problem owing to the diameter of the wire in their modeling. The structure of a warp-knitted wire mesh is very complex, and highly nonlinear contact phenomena occur between the loops and underlaps that cross each other. Li et al. [11] modeled the wire mesh based on fractal mechanics theory and analyzed the mechanical properties of the mesh structure on this basis. Zhu et al. [12] built a finite element model that considered contact by manually searching for contact pairs between wires; however, manually searching for contact pairs only applies to specific structures and is not generalizable.

In this paper, for the modeling of wire mesh, the periodic cubic spline curve is used to describe the space trajectory of the repeating

Received 22 November 2023; revision received 24 December 2023; accepted for publication 27 December 2023; published online 29 January 2024. Copyright © 2024 by the American Institute of Aeronautics and Astronautics, Inc. All rights reserved. All requests for copying and permission to reprint should be submitted to CCC at www.copyright.com; employ the eISSN 1533-385X to initiate your request. See also AIAA Rights and Permissions www.aiaa.org/randp.

*Master, School of Electromechanical Engineering, P.O. Box 191; lizhuolin0721@outlook.com.

†Master, School of Electromechanical Engineering, P.O. Box 191; hanzhang_xd@163.com.

‡Engineer; lys@ipm.com.cn.

§Engineer; wxr@ipm.com.cn.

¶Engineer; tzl@ipm.com.cn.

**Engineer; qyq@ipm.com.cn.

††Professor, School of Electromechanical Engineering, P.O. Box 191; yiqunzhang@xidian.edu.cn (Corresponding Author).

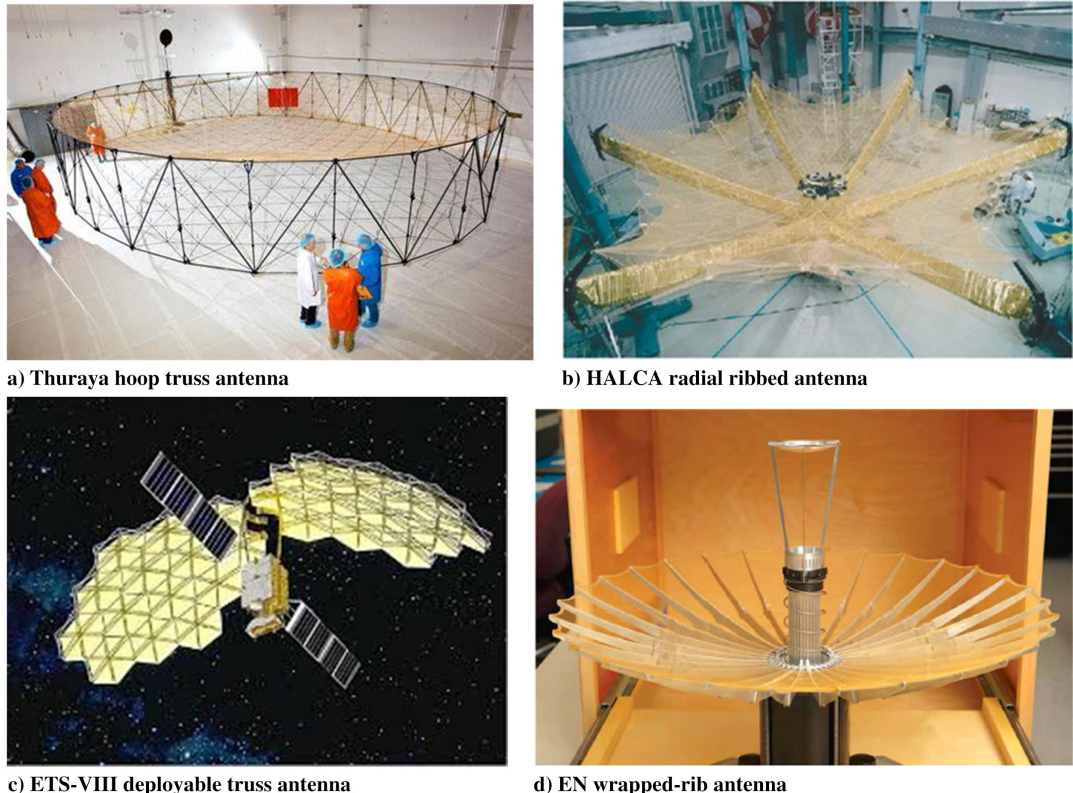


Fig. 1 Deployable mesh reflector antennas.

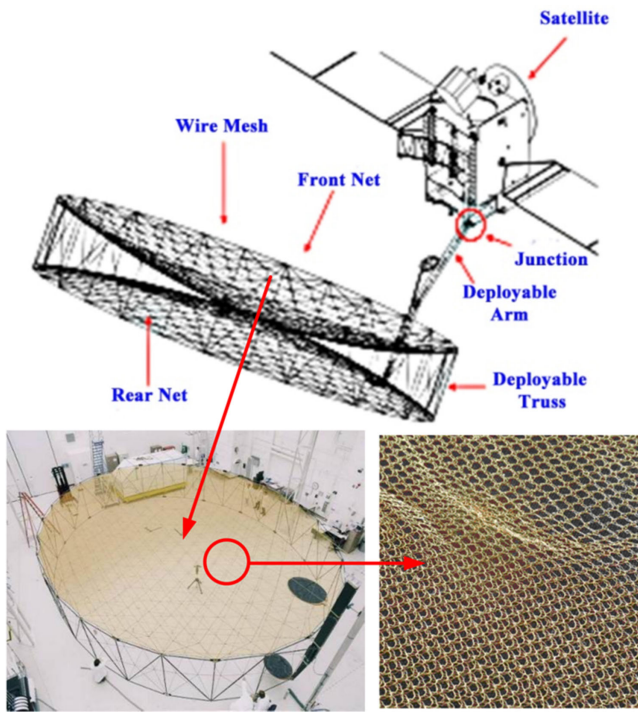


Fig. 2 Wire mesh reflector of the deployable antenna.

unit of the wire mesh structure and to establish the model of the repeating unit of wire mesh. For the inlay problem in the model, a method using sensitivity matrix adjustment is proposed, and its optimization model is established, which in turn can realize the automatic adjustment of the inlay problem of the 3D model of the warp-knitted wire mesh under different parameters. Finally, a complete wire mesh model without an inlay problem was built using vector superposition based on the periodic characteristics of

the wire mesh. For the highly nonlinear contact problem existing in the wire mesh structure, an adaptive matching method for the contact pairs of the finite element model of the wire mesh is proposed, based on which finite element automated modeling and mechanical analysis of the mesh structure are realized to provide a reference for the development and application of warp-knitted wire meshes.

II. Accurate Modeling of Warp-Knitted Wire Mesh

Two key issues must be solved to achieve the 3D geometric model of warp-knitted mesh: the establishment of the repeating unit and inlay adjustment. On the one hand, the monofilament direction of the mesh structure is smooth and has obvious periodicity, and there exists a repeating unit in each warp-knitted structure, which is composed of loops, so the 3D geometric modeling of the wire mesh can start from the loop structure. On the other hand, in the 3D geometric model based on a finite number of control points through high-curve interpolation, after considering the dimensional characteristics of the wire, inlays can occur between the wires, which cannot accurately reflect the geometric structure.

A. Repeating Unit Geometry Model

Warp-knitted fabrics have clear periodic characteristics, and the overall structure of the fabric can be obtained by superposition of the vectors of the repeating units in the horizontal and vertical directions of the fabric. Therefore, establishing a 3D geometric model of warp-knitted fabrics can be simplified to establish a 3D geometric model of its repeating units, and the repeating units are consisted of loops. The two-bar satin wire warp is considered the object of study, whose repeating unit consists of two symmetrical bars (GB1 and GB2), as shown in Fig. 3a, and the structure of a loop is shown in Fig. 3b. The GB1 bar consists of loops ①, ②, ③, and ④. Finally, the loops (1), (2), (3), and (4) of the GB2 bar can be obtained by symmetry transformation. We can study the GB1 and GB2 bars composed of loops to obtain the model of the repeating unit. Therefore, the bar is taken as an example to introduce the method of establishing a 3D geometric model of the repeating unit.

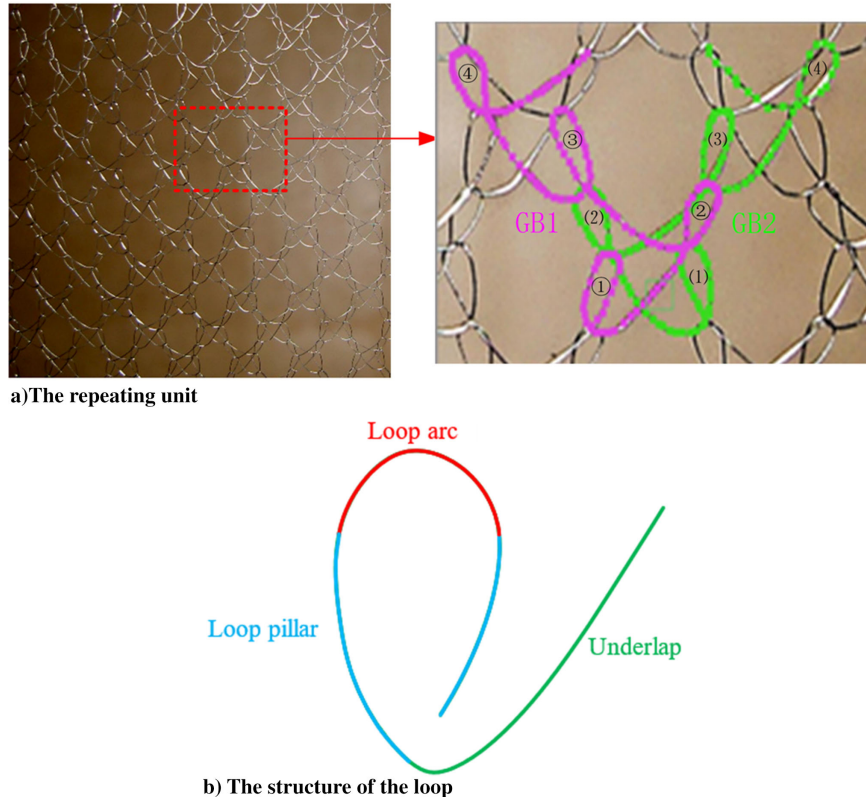
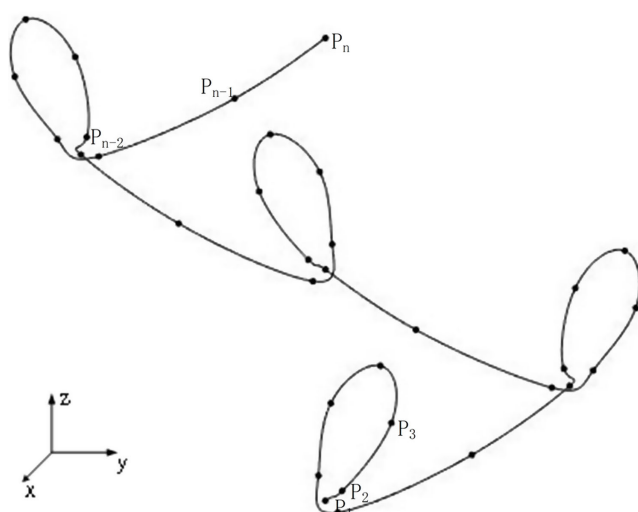


Fig. 3 Two-bar satin wire warp.

1. Repeating Unit Period Cubic Function

The wire goes smoothly in the wire mesh, and so its space trajectory should meet the characteristics of the high-order curve. To achieve a smooth connection of the repeating units, a cubic spline curve is used to describe the repeating units of the wire mesh. The movement diagram and process parameters were assumed to apply to the Cartesian coordinate system. The n control points describing the space pattern of the repeating unit are known as $\mathbf{P}(x, y, z) = \{P_1(x_1, y_1, z_1), P_2(x_2, y_2, z_2), \dots, P_n(x_n, y_n, z_n)\}$, and the complete space trajectory of the repeating unit can be obtained by interpolating the n control points with a periodic cubic spline. Because the GB1 and GB2 bars are symmetrical in space, it is sufficient to study only GB1. The space spline curve of the GB1 bar, as shown in Fig. 4, has n control points that sequentially divide the whole curve into $n - 1$ intervals, and each interval

Fig. 4 Space cubic spline described by n control points.

(between two control points) is a cubic spline curve. The control points of the last three loops are obtained by transforming the first loop.

The cubic spline curve between the two control points was second-order differentiable at each control point. This is expressed on a power basis, as shown in Eq. (1).

$$S(t) = a + b \cdot t + c \cdot t^2 + d \cdot t^3, \quad t \in [0, 1] \quad (1)$$

where $S(t)$ is a cubic function on the normative parameter domain, and a, b, c , and d represent undetermined coefficients.

Because the power base of the parametric cubic spline function is deterministic, to obtain the spatial pattern of the bar, it is only necessary to solve for the coefficients to be determined for the curve $S(t)$.

The large number of repetitive unit control points leads to large calculations of the periodic cubic spline curve interpolation in the normative parameter field. Therefore, it is solved in a non-normative parameter field. We assume an increased sequence $u: u_1 < u_2 < \dots < u_n$ satisfying $\Delta u = u_{i+1} - u_i = 1 (i = 1, 2, \dots, n - 1)$. In the non-normative parameter field $[u_i, u_{i+1}] (i = 1, 2, \dots, n - 1)$, we consider the analytic expression of the $n - 1$ curves as $S_i(u - u_i) (i = 1, 2, \dots, n - 1)$.

In the non-normative parameter field $[u_i, u_{i+1}] (i = 1, 2, \dots, n - 1)$, the parametric equation with the parameter u is shown in Eq. (2).

$$\begin{cases} x = x_i(u - u_i) \\ y = y_i(u - u_i) \\ z = z_i(u - u_i) \end{cases} \quad (2)$$

The specific analytical expressions are given in Eq. (3); for a known $u \in [u_i, u_{i+1}]$, any point on the space curve can be uniquely determined. This point is called the interpolation point.

$$S_i(u - u_i)$$

$$= \begin{cases} x_i(u - u_i) = a_{ix} + b_{ix}(u - u_i) + c_{ix}(u - u_i)^2 + d_{ix}(u - u_i)^3 \\ y_i(u - u_i) = a_{iy} + b_{iy}(u - u_i) + c_{iy}(u - u_i)^2 + d_{iy}(u - u_i)^3 \\ z_i(u - u_i) = a_{iz} + b_{iz}(u - u_i) + c_{iz}(u - u_i)^2 + d_{iz}(u - u_i)^3 \end{cases} \quad i \in (1, 2, \dots, n-1) \quad (3)$$

where $a_{ix}, b_{ix}, c_{ix}, d_{ix}$ ($i = 1, 2, \dots, n-1$) is the undetermined coefficient of the analytical expression for the i th curve.

Periodic boundary conditions satisfy Eq. (4).

$$\begin{cases} \dot{x}_1(u_1 + 0 - u_1) = \dot{x}_{n-1}(u_n - 0 - u_{n-1}) \\ \dot{y}_1(u_1 + 0 - u_1) = \dot{y}_{n-1}(u_n - 0 - u_{n-1}) \\ \dot{z}_1(u_1 + 0 - u_1) = \dot{z}_{n-1}(u_n - 0 - u_{n-1}) \\ \ddot{x}_1(u_1 + 0 - u_1) = \ddot{x}_{n-1}(u_n - 0 - u_{n-1}) \\ \ddot{y}_1(u_1 + 0 - u_1) = \ddot{y}_{n-1}(u_n - 0 - u_{n-1}) \\ \ddot{z}_1(u_1 + 0 - u_1) = \ddot{z}_{n-1}(u_n - 0 - u_{n-1}) \end{cases} \quad (4)$$

where $\dot{x}_1(u_1 + 0 - u_1)$, $\dot{y}_1(u_1 + 0 - u_1)$, and $\dot{z}_1(u_1 + 0 - u_1)$ represent the first derivative in the right neighborhood of $u = u_1$ in the analytic expression of the first curve, and $\dot{x}_{n-1}(u_n - 0 - u_{n-1})$, $\dot{y}_{n-1}(u_n - 0 - u_{n-1})$, and $\dot{z}_{n-1}(u_n - 0 - u_{n-1})$ represent the first derivative in the left neighborhood of $u = u_n$ in the analytic

expression of the last curve. Similarly, there were corresponding secondary derivatives.

In addition, for the non-endpoint control point coordinates in the bar, the continuity must satisfy Eq. (5):

$$\begin{cases} x_{i-1}(u_i - u_{i-1}) = x_i(u_i - u_i) \\ y_{i-1}(u_i - u_{i-1}) = y_i(u_i - u_i) \\ z_{i-1}(u_i - u_{i-1}) = z_i(u_i - u_i) \\ \dot{x}_{i-1}(u_i - u_{i-1}) = \dot{x}_i(u_i - u_i) \\ \dot{y}_{i-1}(u_i - u_{i-1}) = \dot{y}_i(u_i - u_i) \\ \dot{z}_{i-1}(u_i - u_{i-1}) = \dot{z}_i(u_i - u_i) \\ \ddot{x}_{i-1}(u_i - u_{i-1}) = \ddot{x}_i(u_i - u_i) \\ \ddot{y}_{i-1}(u_i - u_{i-1}) = \ddot{y}_i(u_i - u_i) \\ \ddot{z}_{i-1}(u_i - u_{i-1}) = \ddot{z}_i(u_i - u_i) \end{cases} \quad (i = 2, 3, \dots, n-1) \quad (5)$$

From Eq. (3), the $n-1$ curve expression $S_i(u - u_i)$ is uniquely determined by the $12n-12$ undetermined coefficients, so there should be $12n-12$ conditions.

To simplify the description process, in Eq. (3), we chose $x_i(u - u_i) = a_{ix} + b_{ix}(u - u_i) + c_{ix}(u - u_i)^2 + d_{ix}(u - u_i)^3$ as an illustration of the solution, $x_i(u - u_i)$ contains $4(n-1)$ undetermined coefficients. According to Eqs. (2–4), Eq. (6) holds true for $x_i(u - u_i)$.

$$\left\{ \begin{array}{l} 1) \text{start point: } a_{1x} = x_1 \\ 2) \text{non-endpoints: } \begin{aligned} a_{(k-1)x} + b_{(k-1)x} + c_{(k-1)x} + d_{(k-1)x} &= a_{kx} \\ b_{(k-1)x} + 2c_{(k-1)x} + 3d_{(k-1)x} &= b_{kx} \\ 2c_{(k-1)x} + 6d_{(k-1)x} &= 2c_{kx} \end{aligned} \\ 3) \text{end point: } a_{(n-1)x} + b_{(n-1)x} + c_{(n-1)x} + d_{(n-1)x} = x_n \\ 4) \text{boundary conditions: } \begin{aligned} b_{1x} &= b_{(n-1)x} + 2c_{(n-1)x} + 3d_{(n-1)x} \\ 2c_{1x} &= 2c_{(n-1)x} + 6d_{(n-1)x} \end{aligned} \end{array} \right\} \quad (6)$$

where $k = 2, 3, \dots, n-1$

According to Eq. (6), Eq. (7) is obtained.

$$\left\{ \begin{array}{l} \mathbf{A} = [0 \ 0 \ \dots \ 0]_{1 \times 4(n-3)} \\ \mathbf{B} = [1 \ 0 \ 0 \ 0 \ \mathbf{A}]_{1 \times 4(n-2)} \\ \mathbf{C} = \begin{bmatrix} 0 & 0 & 0 & 0 & 1 & 0 & 0 & 0 \\ 1 & 1 & 1 & 1 & -1 & 0 & 0 & 0 \\ 0 & 1 & 2 & 3 & 0 & -1 & 0 & 0 \\ 0 & 0 & 2 & 6 & 0 & 0 & -2 & 0 \end{bmatrix}, \mathbf{D} = \begin{bmatrix} \mathbf{C} & & & \\ & \mathbf{C} & & \\ & & \ddots & \\ & & & \mathbf{C} \end{bmatrix}_{4(n-2) \times 4(n-2)} \\ \mathbf{E} = \begin{bmatrix} 0 & 0 & 0 & 0 \\ 0 & 1 & 0 & 0 \\ 0 & 0 & 2 & 0 \end{bmatrix}, \mathbf{F} = \begin{bmatrix} 1 & 1 & 1 & 1 \\ 0 & -1 & -2 & -3 \\ 0 & 0 & -2 & -6 \end{bmatrix}, \mathbf{G} = [\mathbf{E} \ O]_{3 \times 4(n-2)} \\ \mathbf{H}_x = [a_{1x} \ b_{1x} \ c_{1x} \ d_{1x}, \ a_{2x} \ b_{2x} \ c_{2x} \ d_{2x}, \ \dots, \ a_{(n-1)x} \ b_{(n-1)x} \ c_{(n-1)x} \ d_{(n-1)x}]_{1 \times 4(n-1)}^T \\ \mathbf{J}_x = [x_2 \ 0 \ 0 \ 0, \ x_3 \ 0 \ 0 \ 0, \ \dots, \ x_{n-1} \ 0 \ 0 \ 0]_{1 \times 4(n-2)}, \mathbf{K}_x = [x_1 \ \mathbf{J}_x \ x_n \ 0 \ 0]_{1 \times 4(n-1)}^T \end{array} \right\} \quad (7)$$

Therefore, Eq. (8) is obtained.

$$\mathbf{M}_x \mathbf{H}_x = \mathbf{K}_x \quad (8)$$

Where

$$\mathbf{M}_x = \begin{bmatrix} \mathbf{B} & \mathbf{O} \\ \mathbf{D} & \mathbf{O} \\ \mathbf{G} & \mathbf{F} \end{bmatrix}_{4(n-1) \times 4(n-1)}$$

Because $R(\mathbf{M}_x) = 4(n-1)$, \mathbf{H}_x can be determined uniquely according to Eq. (9).

$$\mathbf{H}_x = \mathbf{M}_x^{-1} \mathbf{K}_x \quad (9)$$

\mathbf{H}_x represents the $4(n-1)$ coefficients of $x_i(u - u_i)$. Similarly, the $4(n-1)$ coefficients to be determined from the expressions for $y_i(u - u_i)$ and $z_i(u - u_i)$ can be obtained using Eqs. (10) and (11), respectively.

$$\mathbf{H}_y = \mathbf{M}_y^{-1} \mathbf{K}_y \quad (10)$$

$$\mathbf{H}_z = \mathbf{M}_z^{-1} \mathbf{K}_z \quad (11)$$

where $\mathbf{H}_y = [\mathbf{H}_{y1} \ \mathbf{H}_{y2} \ \dots \ \mathbf{H}_{y(n-1)}]^T$, $\mathbf{H}_z = [\mathbf{H}_{z1} \ \mathbf{H}_{z2} \ \dots \ \mathbf{H}_{z(n-1)}]^T$, $\mathbf{H}_{yi} = [a_{iy} \ b_{iy} \ c_{iy} \ d_{iy}]^T$, and $\mathbf{H}_{zi} = [a_{iz} \ b_{iz} \ c_{iz} \ d_{iz}]^T$ ($i = 1, 2, \dots, n-1$).

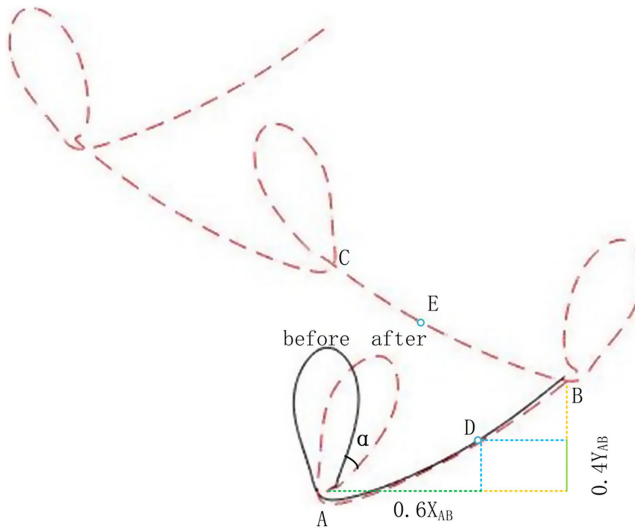


Fig. 5 Tilt of the loop.

Let $\mathbf{H}_x = [\mathbf{H}_{x1} \ \mathbf{H}_{x2} \ \dots \ \mathbf{H}_{x(n-1)}]^T$, then $\mathbf{H}_{xi} = [a_{ix} \ b_{ix} \ c_{ix} \ d_{ix}]^T$ ($i = 1, 2, \dots, n-1$). $\mathbf{U} = [1 \ (u - u_i) \ (u - u_i)^2 \ (u - u_i)^3]$, and so we can obtain Eq. (12).

$$\begin{aligned} S_i(u - u_i) &= [x_i(u - u_i) \ y_i(u - u_i) \ z_i(u - u_i)] \\ &= [\mathbf{UH}_{xi} \ \mathbf{UH}_{yi} \ \mathbf{UH}_{zi}] \end{aligned} \quad (12)$$

where $i = 1, 2, \dots, n-1$.

In summary, the space trajectory equation of the central axis of the bar can be determined using Eq. (12). The coordinates of any interpolation point on $S_i(u - u_i)$ can be obtained by arbitrarily assigning $u = u_j$ and $u_j \in [u_1, u_n]$ ($n \geq 4, j = 1, 2, \dots, n-1$).

2. Tilted Loop Model

However, the above process was deduced for an ideal case. In actual knitting, the underlap is subjected to a force that is not parallel to its axial direction at the contact point with the neighboring loop, resulting in tilting deformation of the loop [13,14]. Rotation of the control points was used to ensure the accuracy of the 3D geometric model of the wire mesh. The rotation matrix is expressed by Eq. (13), where α represents the deflection angle.

$$T_1 = \begin{bmatrix} \cos \alpha & -\sin \alpha & 0 & 0 \\ \sin \alpha & \cos \alpha & 0 & 0 \\ 0 & 0 & 1 & 0 \\ 0 & 0 & 0 & 1 \end{bmatrix} \quad (13)$$

As shown in Fig. 5, the tilt of the loop generally occurs in the loop arc and pillar, and the underlap can be determined based on their positions. For the tilt part, the coordinates of the related values are multiplied by the rotation matrix Eq. (13). Points D and E on the underlap are located between starting points A and B, and their positions can be taken as $(0.6X_{AB}, 0.4Y_{AB})$, the z coordinate remains unchanged.

Based on the above theory, the space-trajectory control points describing the length direction of the wire mesh can be derived, the space trajectory can be determined, and the initial 3D geometric model of the repeating unit with dimensional characteristics can be obtained using a circle of diameter D to sweep along the space-trajectory curve. Select the wire diameter $D = 0.05$ mm and loop tilt angle $\alpha = 20^\circ$, and the CAD model of the repeating unit of the two-bar satin is established, as shown in Fig. 6.

B. Adjustment of Inlay

The modeling approach described in the previous section does not consider the diameter of the wire, which is likely to create inlay

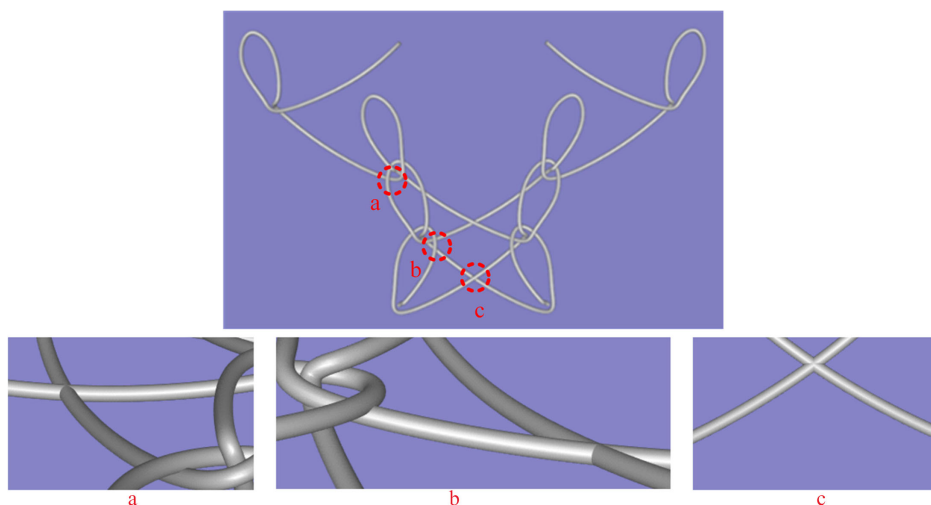


Fig. 6 CAD model of the repeating unit.

problems when the wires are adjacent to each other, as shown in Figs. 6a–6c. However, the 3D model established in this study has certain disadvantages. First, it cannot completely restore the spatial geometry of the wire mesh, and, second, nonlinear contacts exist between the loops and underlaps, which are key factors affecting the mechanical properties of the wire mesh structure. The finite element model established based on this geometrical model cannot be accurately analyzed for contact problems. To avoid this problem, the practice in previous studies was to manually adjust the controlled point coordinates describing the loop. However, this method lacks theory, requires many control point coordinates to be adjusted each time, and results in mutual interference of the adjustment effects, requiring multiple adjustments. Therefore, to solve the inlay problem, this study proposes a method using a sensitivity matrix adjustment and develops an optimization model.

1. Determination Principle of Inlay

The repeating unit of the two-bar satin described by the periodic cubic spline curves consists of the curve $S_1 \sim S_{64}$; $S_1 \sim S_{32}$ is the curve for the GB2 bar, and $S_{33} \sim S_{64}$ is the curve for the GB1 bar, as shown in Fig. 7, where $S'_i (1 < i < 64)$ denotes the curve after translation of the repeating unit. The contact position of the wire mesh can be divided into two main categories: The contact between wires in the repeating unit, the set of contact positions is noted as ψ_1 , such as the contact between the curve and the curve S_{39} . The contact between the wire of the repeating unit and the wire of the neighboring repeating unit, the set of contact positions is noted as ψ_2 , such as the contact between the curve S_{23} and the curve S'_{55} . The curves on the repeating unit are collectively noted as S , and the curves around the repeating unit are noted as S' ; then the contact position of the wire can be determined by Eq. (14).

$$\psi_1 = S_i \cap S_j (i, j = 1, 2, \dots, 64, i \neq j)$$

$$\psi_2 = S_k \cap S'_h \left(\begin{array}{l} k = 1, 2, \dots, 64 \\ h = 2, 10, 16, 18, 19, 20, 22, 23, 24, 26, 30, \\ 31, 32, 43, 44, 47, 51, 52, 56, 59, 60, 62, 63 \end{array} \right) \quad (14)$$

As the expression of the repeating unit curve is a cubic power function with parameters, the solution of the two intersecting curves is not unique, and it is difficult to confirm the contact location. Therefore, several serial interpolation points on the cubic spline curve of the repeating unit were used to determine the inlay extent of the wire contact positions. The contact positions of the two intersecting curves can then be determined using the nearest points on the xoy projection surface, such as points a and b, as shown in Fig. 8. The extent of the inlay can be calculated quantitatively using the z coordinates of the nearest interpolation points at each contact position

Based on the z coordinates of the interpolation points at the contact position, it was possible to determine whether an inlay existed between the wires and the extent of the inlay. Mark the initial z coordinates of the wires above the contact position as z_{up} and those below the contact position as z_{down} . Subsequently, the method of judgment is as follows:

1) If $D < \Delta z$ holds, it shows no inlay at the contact position, and no adjustment needed.

2) If $D > \Delta z$ holds, it shows inlay at the contact position.
where $\Delta z = |z_{\text{up}} - z_{\text{down}}|$ represents the distance between the central axes of the upper and lower wires at the contact position.

For the inlay at the contact position, the method of quantitative adjustment is as follows:

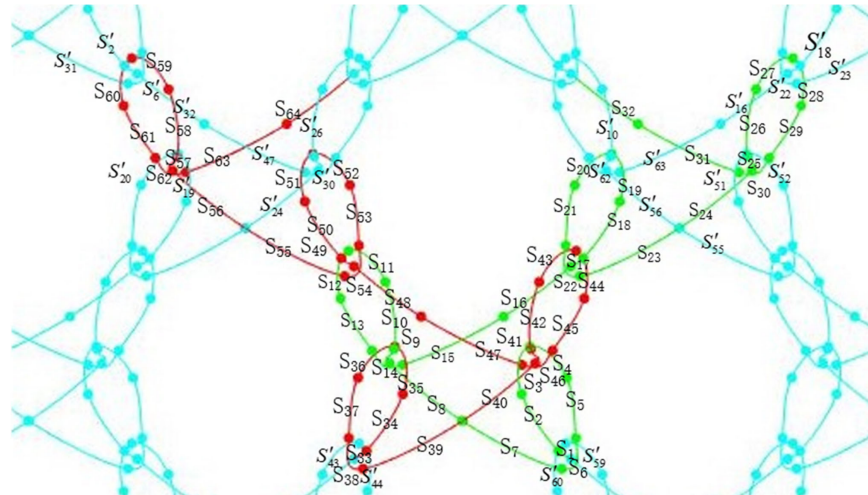


Fig. 7 Schematic of intersecting curves.

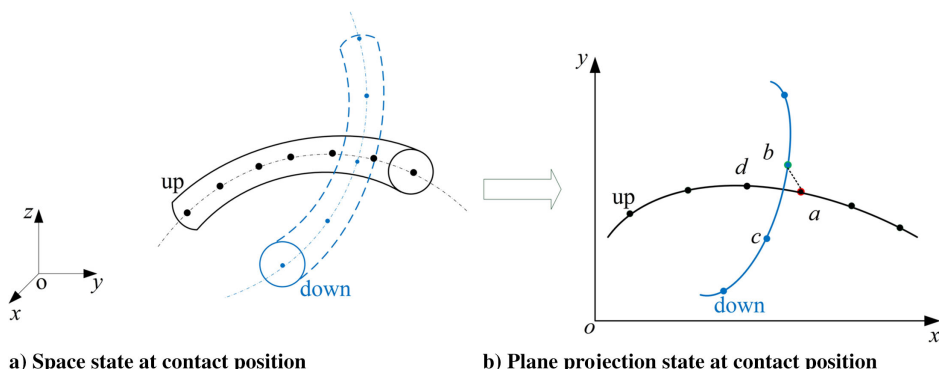


Fig. 8 Interpolation points up and down of wire at the contact position.

1) If $0 < z_{\text{up}} - z_{\text{down}} < D$ holds, let $z'_{\text{up}} = z_{\text{up}} + h$.

2) If $-D < z_{\text{up}} - z_{\text{down}} < 0$ holds, let $z'_{\text{down}} = z_{\text{down}} - h$.

where D is the wire diameter; z_{up} and z'_{up} represent the coordinates of the central axis of the upper wire before and after the adjustment, respectively; z_{down} and z'_{down} represent the coordinates of the central axis of the lower wire before and after adjustment, respectively; and h is the adjustment amount because the diameter of the wire is very thin and can be expressed as Eq. (15).

$$h = \mu D \quad (15)$$

where μ is a settable value, and $\mu \ll 1$.

2. Adjustment Model of Initial Control Points

Because the interpolation points for judging inlay and adjustment amount are based on the coordinates of control points interpolated by period cubic spline curves, the positions of the interpolation points are directly related to the coordinates of the control points, and the distance between control points can be judged automatically. Then, the adjustment amount can be calculated by automatic optimization to eliminate the inlay. To simplify the adjustment, the x and y coordinates of the initial control point were kept unchanged, and only the z coordinates of the control point were adjusted. Simultaneously, based on the smooth connection between the repeating unit models, the z coordinates of the first and last control points should remain unchanged, and only the control points of the non-endpoints should be adjusted. This adjustment is given by Eq. (16).

$$\begin{aligned} \text{Find } \Delta P^z &= (\Delta P_2^z, \Delta P_3^z, \dots, \Delta P_{n-1}^z)^T \\ \text{Min } f &= \sum |K^s| \\ \text{S.t. } |\Delta z| &- D > \delta D \end{aligned} \quad (16)$$

The design variables, objective function, and constraints are as follows:

1) Design variables: The change in the z coordinates of any control point affects the contact state between wires; therefore, the extent of inlay between wires is a function of the variable of the z coordinates of all control points. Therefore, the design variables are the adjusted amounts of the z coordinates of the non-endpoints and can be expressed as $\Delta P^z = (\Delta P_2^z, \Delta P_3^z, \dots, \Delta P_{n-1}^z)^T$, and n is the total number of control points.

2) Objective function: The optimization goal is to obtain a structure without an inlay between wires; therefore, the objective function can be described as minimizing the sum of the absolute values of the inlay adjustment, with K^s representing the amount of inlay adjustment for the position s .

3) Constraints: To ensure that no inlay exists around the contact position, the contact position should satisfy $\Delta z - D > \delta D$, where $\delta \in (0, 1)$ means that the z coordinates between the two interpolation points used to judge the inlay are larger than one wire diameter and smaller than two.

3. Solving the Adjustment Model

It can be observed that the amount of inlay adjustment is less than the wire diameter from Eq. (15); thus, it is small relative to the size of the repeating unit. Therefore, the adjustment problem can be linearized using Eq. (17).

$$S \cdot \Delta P^z = K^s \quad (17)$$

where ΔP^z is the adjustment amount of the z coordinates of the control points, and S is the sensitivity matrix, which represents the variable of the adjustment amount relative to the variable of the z coordinates of the control points, as shown in Eq. (18).

$$S = \begin{bmatrix} \frac{\partial K_2^1}{\partial P_2} & \frac{\partial K_3^1}{\partial P_3} & \dots & \frac{\partial K_{n-1}^1}{\partial P_{n-1}} \\ \frac{\partial K_2^2}{\partial P_2} & \frac{\partial K_3^2}{\partial P_3} & \dots & \frac{\partial K_{n-1}^2}{\partial P_{n-1}} \\ \vdots & \vdots & \ddots & \vdots \\ \frac{\partial K_2^s}{\partial P_2} & \frac{\partial K_3^s}{\partial P_3} & \dots & \frac{\partial K_{n-1}^s}{\partial P_{n-1}} \end{bmatrix}_{s \times (n-2)} \quad (18)$$

where $K_i^j (i = 2, 3, \dots, n-1; j = 1, 2, \dots, s)$ represents the amount of change at s inlay caused by an increment ΔP of the i th control point.

The sensitivity matrix S in Eq. (18) is expressed as follows: It is assumed that the z coordinate of the control point is ΔP_0^z in the initial structure, and its adjustment is K^s . An incremental ΔP of z coordinates of non-endpoint control points at each time and a periodic cubic spline curve correspondingly fit these changed control points. Therefore, the inlay amount is changed simultaneously, and the variable of the adjustment amount is marked as ΔK . Finally, each element of the sensitivity matrix S is calculated using $\partial K / \partial P$.

This process was repeated until the inlay was not in the structure. The z coordinate adjustment amount ΔP^z of the control points can be determined, as expressed by Eq. (19).

$$\Delta P^z = S^{-1} \cdot K^s \quad (19)$$

The z coordinates of the adjusted control points can be expressed using Eq. (20).

$$P_{\text{adjust}}^z = P_0^z + \Delta P^z \quad (20)$$

where P_0^z is the z coordinate of the initial geometric model.

Therefore, $(P_0^x, P_0^y, P_{\text{adjust}}^z)$ was the control point of the adjusted 3D geometric model. P_0^x and P_0^y represent the x and y coordinates of the initial geometric model, respectively.

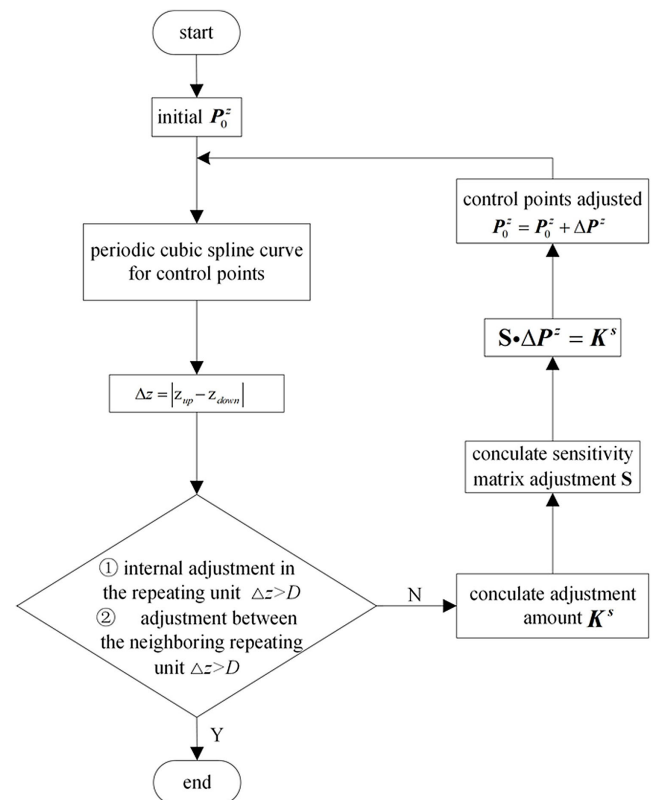


Fig. 9 The adjustment flowchart.

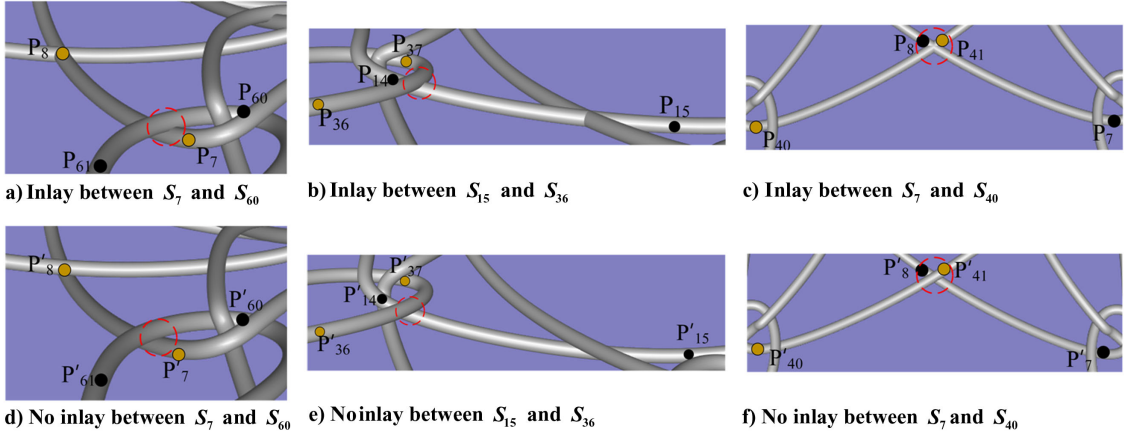


Fig. 10 Comparison of inlay adjustment.

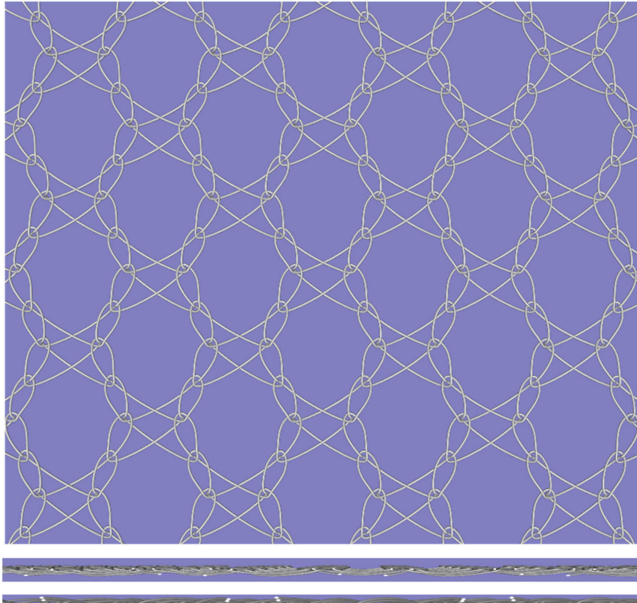


Fig. 11 The overall structure of the two-bar satin wire warp.

The adjustment flowchart and optimization process are shown in Fig. 9.

where $\delta = 0.05$ is considered the constraint. Obtaining new control points from the adjustment results. Based on the new control points, we can obtain the 3D geometric model of the repeating unit without an inlay between the wires, as shown in Fig. 10.

C. Model of the Overall Wire Mesh

Furthermore, based on the periodic characteristics of the warp-knitted wire mesh and using Eq. (21), the overall structure can be obtained by vector superposition of the repeating units.

$$\begin{aligned} \mathbf{P} &= \mathbf{P}_0 + a_0 \mathbf{R}_x + a_1 \mathbf{R}_y, \\ |a_i| &\in (0, \infty), |a_i| \in \mathbb{Z}, (i = 0, 1, 2) \end{aligned} \quad (21)$$

where \mathbf{P}_0 is the repeating unit, \mathbf{P} is the overall structure, and \mathbf{R}_x and \mathbf{R}_y are the horizontal and vertical repetition vectors of the wire mesh. The overall structure of the two-bar satin wire warp is illustrated in Fig. 11.

III. Finite Element Modeling of Wire Mesh Considering Contact Problems

An accurate finite element model is a prerequisite for verifying the mechanical properties that directly affect the accuracy and reliability

of simulation results. Finite element modeling of the wire mesh considers two major issues. The highly nonlinear contact phenomena between the loops and underlaps intersect. The 3D geometric model of the wire mesh structure established in the previous section is relatively complex, and to simplify the finite element model, the interpolation points describing the 3D geometric model must be requested on demand.

A. Automatic Determination of Contact Pairs in Wire Mesh Structures

Previous researchers have manually searched for contact pairs between wires; however, the method is not generalizable. In this study, an adaptive matching method was proposed to find the contact pair of the finite element model of the wire mesh.

The contact in the two-bar satin wire warp can be divided into two categories: The contact between loops and three contact pairs can be created for modeling: between curve ac and bd, between curve ad and ac, and between curve bd and ad. The contact between underlaps that cross each other is established using curve ig with curve fh. The details are shown in Fig. 12.

It can be observed from Fig. 12, where a–e are the locations of direct contact between the wires. Therefore, contact pairs can be established by searching for direct contact points between the wires. Using the same principle of searching for the contact position between wires as in Sec. II, the direct contact point can be determined by the nearest interpolation points on its two intersecting curves. The period cubic spline curve describing the central axis of the wire mesh is discretized into an infinite number of points, and the number of interpolation points on each section of the curve is denoted as num-points, which are numbered sequentially according to the sequential direction of the control point. The search results are shown in Fig. 13a.

Because the interpolation points are discrete, searching for the two nearest neighboring interpolation points on the intersecting curves S_1 and S_2 does not necessarily satisfy $(x_{S_i} - x_{S_j})^2 + (y_{S_i} - y_{S_j})^2 = 0$, and the search will likely lead to the case shown in Figs. 14a and 14b. Incorrect contact area of contact pairs established in this case can result in inaccurate finite element modeling of the wire mesh, causing errors in the simulation results and even leading to nonconvergence of the results. Moreover, the aforementioned method searches for only one contact point at the underlap and does not define the contact pair. Therefore, we need to improve these points, and the improvement of the contact points is divided into two parts:

1) Contact-point improvement at the loops: The interpolation points in its neighborhood were searched as endpoints to expand the contact area to define the contact pairs.

2) Contact-point improvement at the underlaps: The contact point was used as a reference to search for neighboring interpolation points toward both ends as endpoints to define contact pairs.

The number of search interpolation points can be set to 0.1 times num-points on each curve section. The improved contact points are shown in Fig. 13b. The contact pairs of each part of the mesh structure

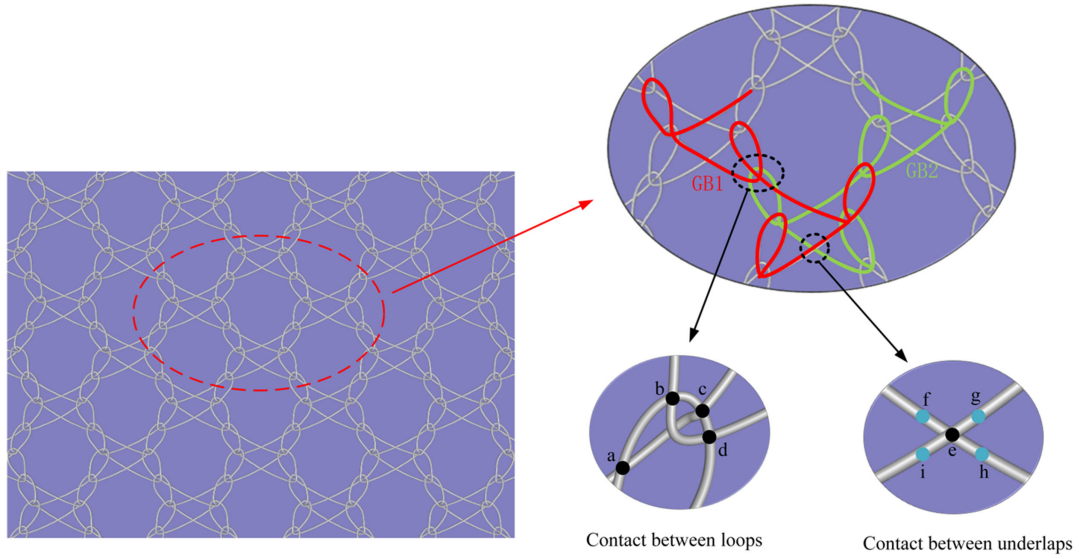


Fig. 12 The contact in the two-bar satin wire warp.

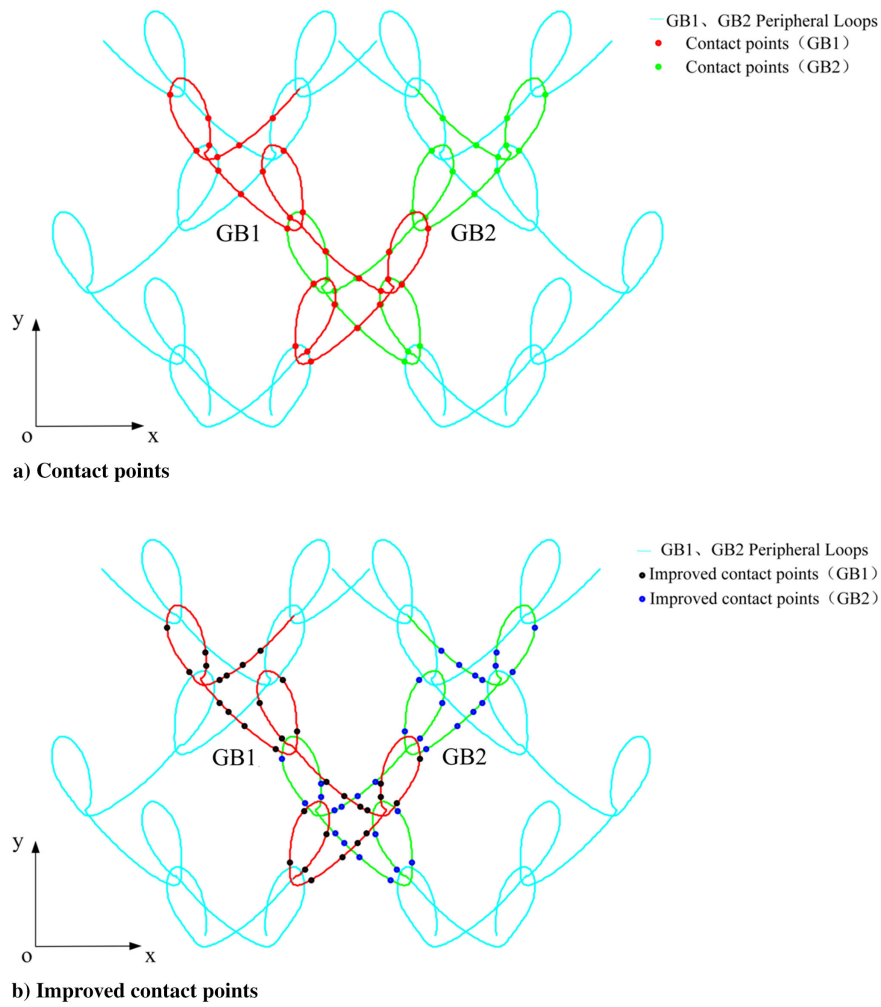


Fig. 13 Contact points of the repetitive unit.

are defined according to the improved contact points, as shown in Fig. 15.

B. Automated Finite Element Modeling

The above has been searched for relevant interpolation points that can be used as key points to describe the finite element model of the wire mesh; however, the points on the contact pairs are insufficient to

describe the mesh structure. Therefore, more interpolation points must be selected for accurate finite element modeling of the wire mesh. The wire mesh loop is characterized by a large curvature of the loop arc, a small curvature of the loop pillar, and the underlap, such that the number of key points can be selected according to the size of the curvature. The curvature of the space curve $S(t)$, which contains parameter t , can be expressed as Eq. (23).

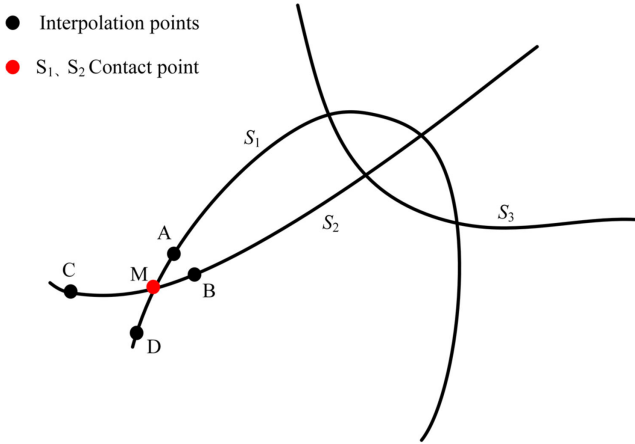


Fig. 14 Incorrect interpolation points search case.

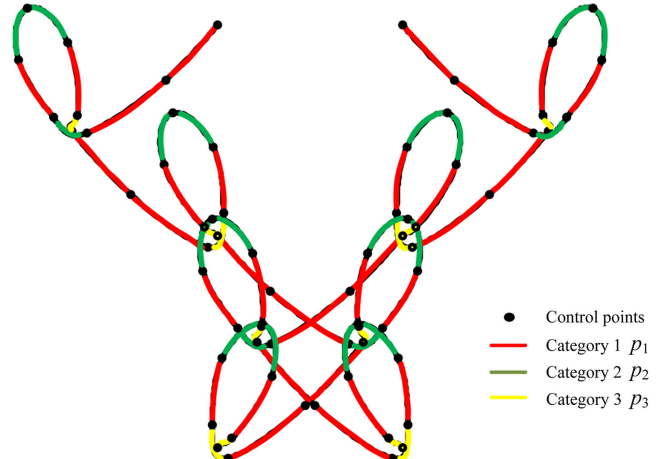


Fig. 16 Repeating unit curvature classification.

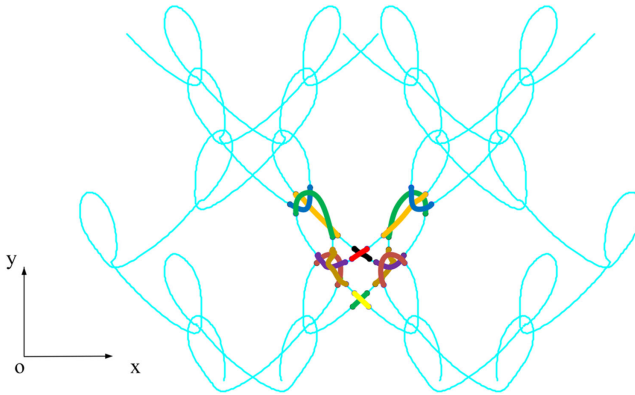


Fig. 15 Contact pairs in the mesh structure.

$$S(t) = \begin{cases} x = x(t) \\ y = y(t) \\ z = z(t) \end{cases} \quad (22)$$

$$K = \frac{\sqrt{|p|^2|q|^2 - (p \cdot q)^2}}{|v|^3} \quad (23)$$

where $p = \sqrt{(x'(t))^2 + (y'(t))^2 + (z'(t))^2}$ and $q = \sqrt{(x''(t))^2 + (y''(t))^2 + (z''(t))^2}$.

Combining the characteristics of the large curvature of the loop arc, the small curvature of the loop pillar, and the underlap, the curves can be classified into three, as shown in Fig. 16, with the following criteria:

$$\begin{cases} p_1: K_{\max} \in (0, 8] \\ p_2: K_{\max} \in (8, 13] \\ p_3: K_{\max} \in (13, 62] \end{cases}$$

where K_{\max} is the maximum curvature.

As shown in Fig. 17, the selection of the key points based on the maximum curvature difference of the curve can be described as follows: First, between the curved section defined by two neighboring control points A and B, interpolation point 1 is obtained in the middle of the two control points; then, using the control point and this interpolation point as the initial points, interpolation points 2 and 3 are obtained in the same way; finally, the above process is repeated several times to obtain the desired key points describing any curve. When the maximum curvature range of the repeating unit curve is (0,8], the above process is repeated twice; the process is repeated three times when the range is (8,13]; the process is repeated four times

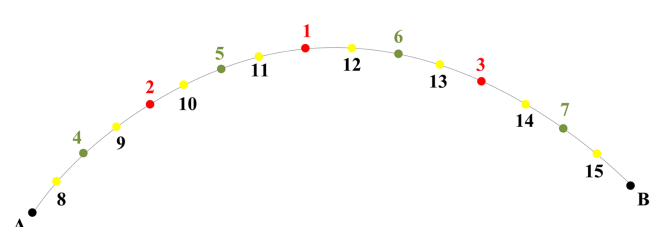


Fig. 17 Selection of interpolation points.

in the range (13,62]. The key points of the finite element model describing each section of the curve were obtained.

The improved contact points and key points selected on different curvature curves were finally used for all the key points of the finite element model, as shown in Fig. 18.

The wire material is defined as a beam unit. The shape of the beam unit is a circle, and the diameter of the circle is 0.05 mm, which is the same as the diameter of the wire. The finite element model of the wire mesh considering the contact problem is established, as shown in Fig. 19. The contact pairs in the model are shown in Fig. 20.

IV. Simulation Analysis and Experimental Comparison

To verify the accuracy of our finite element model of the wire mesh, we performed a simulation analysis and physical experiments on bidirectional stretching with a square wire mesh of 1 m × 1 m size.

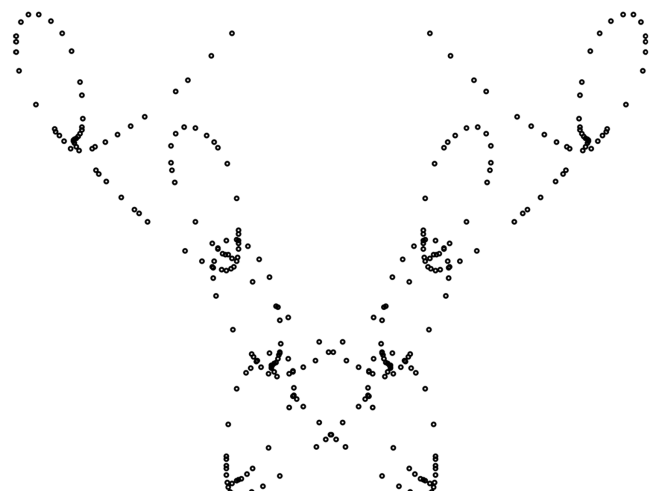


Fig. 18 All key points of the finite element model.

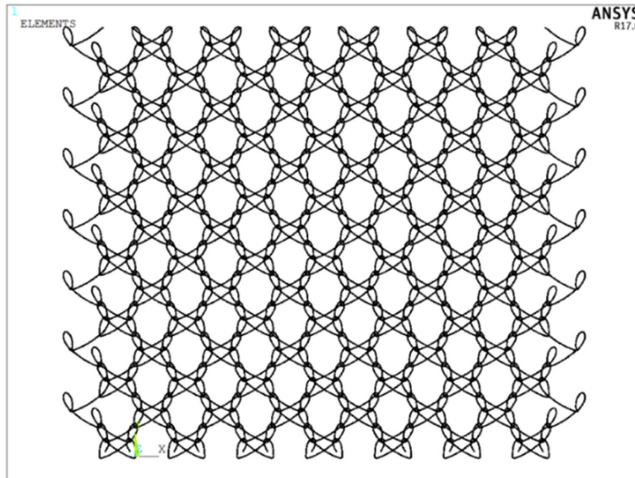


Fig. 19 The finite element model of wire mesh.

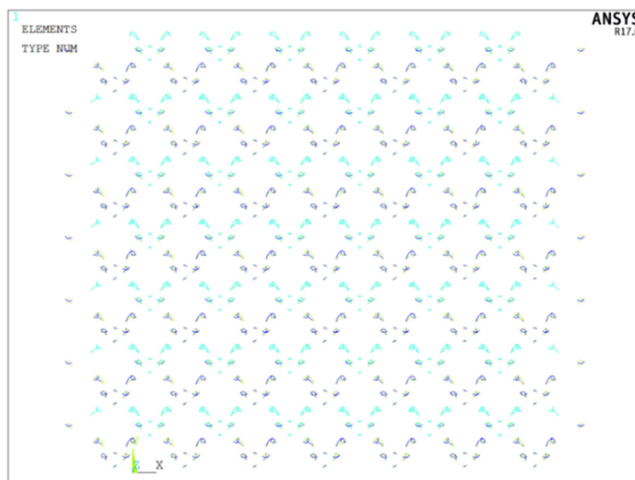


Fig. 20 The contact pairs in the finite element model.

A. Mechanical Simulation Analysis of the Wire Mesh Structure

Assuming that the wire mesh is stretched by a bidirectional load F_X and F_Y , deformation occurs, as shown in Fig. 21, and strain occurs in the transverse and longitudinal directions of the wire mesh, where point A corresponds to the fully constrained point of the finite element model.

The mesh parameters for the bidirectional stretching mesh experiment were as follows: two-bar satin wire warp organization and nickel-plated stainless-steel wire. The height of the loop was 1 mm, the course spacing was 3.63 mm, the tilt angle of the loop was 20°, the diameter was 0.05 mm, Poisson's ratio was 0.3, and the modulus of elasticity was 726.2 MPa.

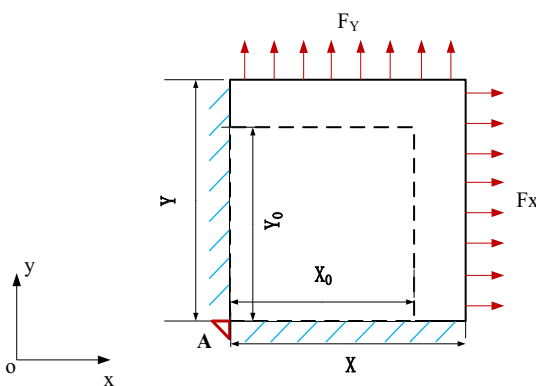


Fig. 21 The deformation of the wire mesh.

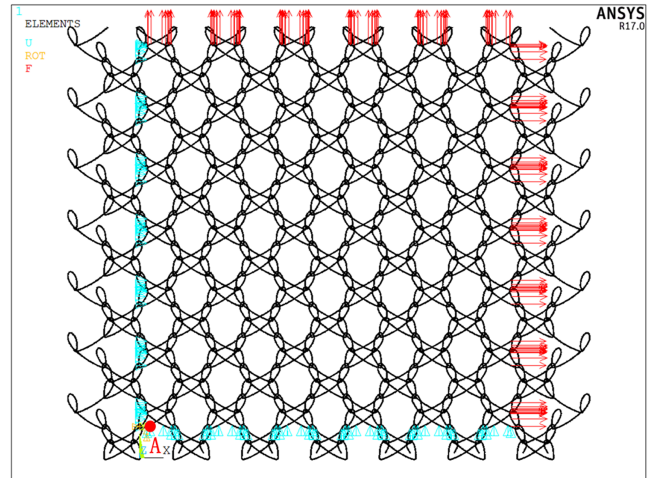


Fig. 22 Load on the wire mesh.

Based on the finite element model in Sec. III, the boundary conditions and load directions are shown in Fig. 22, where the full constraint is at point A and the load is 15–50 N/m. The theoretical transverse and longitudinal strain results for the wire mesh obtained using this model are presented in Table 1.

B. Wire Mesh Bidirectional Stretching Test

The bidirectional stretching experiment of wire mesh is shown in Fig. 23, and the experimental steps are as follows: ①, five pieces of two-bar satin wire warp of the same size were taken and placed on the experimental bench; ②, a 15 N weight was placed around the mesh as the initial load, and then 5 N weights were added around the mesh in seven steps later to realize the loading from the initial 15 to 50 N/m, and bidirectional stretching experiments were carried out for the longitudinal strain range of 10–20%; ③, after adding weights each time and waiting for the mesh to stabilize in stretch, its elongation was measured in the transverse and longitudinal directions; ④, the above experimental process was repeated for five mesh samples, the transverse and longitudinal elongations of the mesh under different working conditions were measured, the average value was taken as the final result, and the strain was calculated according to the strain formula.

The experimental data are listed in Table 1, and a comparison of the simulation and experimental results is shown in Fig. 24.

The following can be seen in the table and figure:

1) By comparing the numerical simulation data with the experimental data, the maximum error of the transverse strain during the bidirectional stretching of the mesh was 5.71%, and the maximum error of the longitudinal strain was 4.07%. The data verify the effectiveness of the automated modeling and simulation analysis method proposed in this study.

2) When the transverse and longitudinal sizes of the mesh were the same and subjected to the same load, the transverse strain was greater than the longitudinal strain, showing an apparent anisotropy, in which the transverse strain was slightly more significant than the longitudinal strain. The transverse-to-longitudinal strain ratio is between 1.6 and 2.2 times in the linear elastic range, and the gap between the transverse and longitudinal strains increases with the increase of load, so the anisotropic properties of the mesh become more evident with the increase of load in the linear elastic range.

V. Conclusions

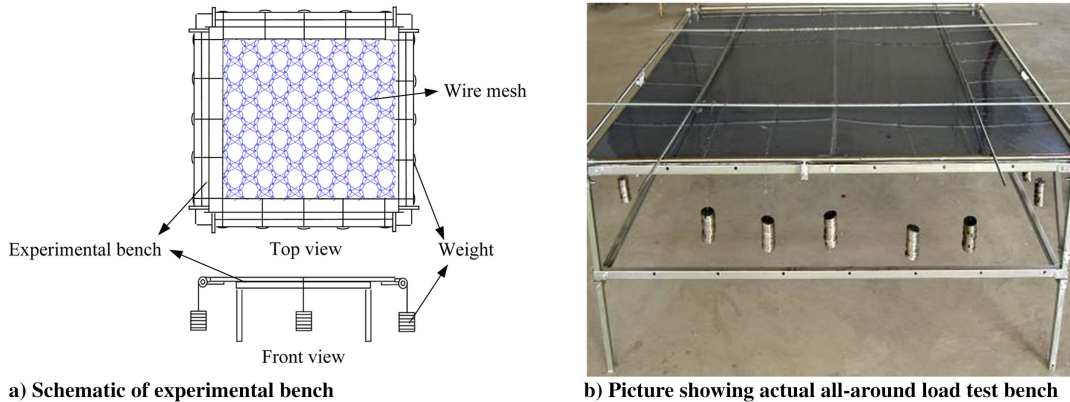
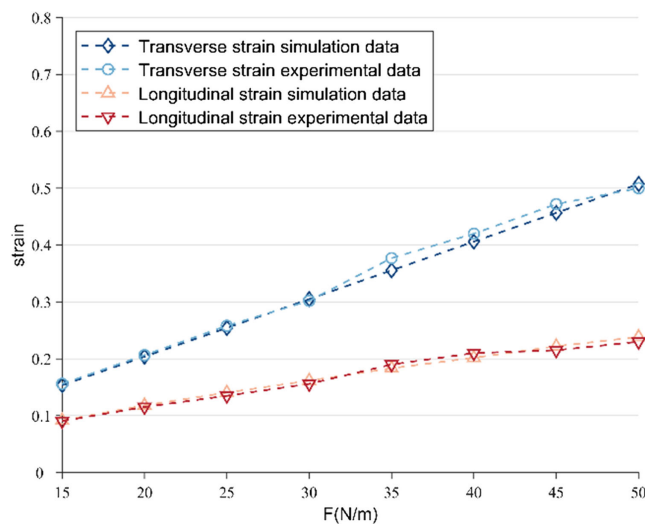
This study focused on accurate 3D geometric modeling of a warp-knitted mesh and finite element modeling considering the contact problem, which can be summarized as follows:

1) Accurate 3D geometric modeling of warp-knitted mesh structures: A periodic cubic spline function describing the repeating unit of the wire mesh was derived, and the control points of the loop were adjusted by considering the tilting of the loop due to the uneven force,

Table 1 Comparison of the simulation results with the experimental results

Loads, N/m	Transverse strain			Longitudinal strain		
	Simulation data	Experimental data	Error, %	Simulation data	Experimental data	Error, %
15	0.1535	0.1560	1.63	0.0915	0.0905	1.12
20	0.2037	0.2064	1.30	0.1181	0.1152	2.52
25	0.2543	0.2581	1.47	0.1405	0.1350	4.07
30	0.3049	0.3020	0.95	0.1615	0.1560	3.52
35	0.3555	0.3770	5.71	0.1834	0.1900	3.48
40	0.4061	0.4200	3.32	0.2018	0.2100	3.92
45	0.4566	0.4720	3.25	0.2220	0.2150	3.27
50	0.5072	0.5000	1.44	0.2384	0.2300	3.64

Bold numbers ment the max error.

**Fig. 23 Schematic diagram of bidirectional stretching experiment.****Fig. 24 Comparison curve between theoretical and experimental data.**

based on which the initial geometrical model of the wire mesh was established. Aiming at the inlay problem of wire contacts in the model, we propose a method using the sensitivity matrix adjustment and establish its optimization model. Finally, the overall accurate 3D geometric modeling of the mesh was completed by vector superposition of the repeating units in the horizontal and vertical directions.

2) Automated finite element modeling for contact problems. Based on an accurate 3D geometric model and its structural characteristics, a set of automated determination and establishment methods for contact pairs is proposed. We selected the key points describing the repeating units by combining the characteristics of the large curvature of the loop arc, the slight curvature of the loop pillar, and the underlap. Based on these critical points, we realized the automatic construction of the finite element model for contact problems. Using the finite element model to simulate the mechanical properties of mesh stretching and, finally, through actual mesh stretching experiments, the

theoretical and experimental data were compared to verify the accuracy of the finite element model.

Acknowledgments

This work was supported by the National Natural Science Foundation of China (No. U2241247), the Scientific and Technological Project of Yunnan Precious Metals Laboratory (YPML-2023050244), the academician expert workstation of Yunnan (No. 202305AF150170) and the Fundamental Research Funds for the Central Universities.

References

- [1] Duan, B.-Y., "The State-of-the-Art and Development Trend of Large Space-Borne Deployable Antenna," *Electro-Mechanical Engineering*, Vol. 33, No. 1, 2017, pp. 1–14.
- [2] Akira, M., Kyoji, S., Motofumi, U., and Akio, T., "In-Orbit Deployment Characteristics of Large Deployable Antenna Reflector Onboard Engineering Test Satellite VIII," *Acta Astronautica*, Vol. 65, Nos. 9–10, 2009, pp. 1306–1316.
- [3] Zhang, Y., Zhang, H., Yang, D., Qin, Q., and Zhu, R., "Form-Finding Design of Cable-Mesh Deployable Reflector Antennas Considering Wire Mesh Properties," *AIAA Journal*, Vol. 57, No. 11, 2019, pp. 5027–5041. <https://doi.org/10.2514/1.J058213>
- [4] Goktepe, O., "Use of Non-Uniform Rational B-Splines for Three-Dimensional Computer Simulation of Warp Knitted Structures," *Turkish Journal of Engineering & Environmental Sciences*, Vol. 25, No. 4, 2001, pp. 369–378.
- [5] Goktepe, O., "HARLOCK S C. A 3D Loop Model for Visual Simulation of Warp-Knitted Structures," *Journal of the Textile Institute*, Vol. 93, No. 1, 2002, pp. 11–28. <https://doi.org/10.1080/00405000208630549>
- [6] Goktepe, O., and Harlock, S. C., "Three Dimensional Computer Modelling of Warp Knitter Structures," *Textile Research Journal*, Vol. 72, No. 3, 2002, pp. 266–272. <https://doi.org/10.1177/004051750207200314>
- [7] Cong, H., Ge, M., and Jiang, G., "3-D Modeling for Warp Knitted Fabric Based on NURBS," *Journal of Textile Research*, Vol. 29, No. 11, 2008, pp. 132–136.

- [8] Jiang, G., Gu, L., Cong, H. L., Miao, X. H., Zhang, A., and Gao, Z., “Geometric Model for Multi-Axial Warp-Knitted Fabric Based on NURBS,” *Fibers & Textiles in Eastern Europe*, Vol. 105, No. 3, 2014, pp. 91–97.
- [9] Xu, H., Jiang, J., and Chen, N., “3D Simulation of Warp-Knitted Structure Based on TexGen,” *Journal of Textile Research*, Vol. 36, No. 3, 2015, pp. 140–146.
- [10] Xu, H. Y., Chen, N. L., Jiang, J. H., Jin, L. X., and Wang, Z. X., “3D Simulation of Warp Knitted Structures with a New Algorithm Based on NURBS,” *Fibres & Textiles in Eastern Europe*, Vol. 23, No. 1, 2015, pp. 57–60.
- [11] Li, T., Jiang, J., Shen, T., and Wang, Z., “Analysis of Mechanical Properties of Wire Mesh for Mesh Reflectors by Fractal Mechanics.” *International Journal of Mechanical Sciences*, Vol. 92, March 2015, pp. 90–97.
<https://doi.org/10.1016/j.ijmecsci.2014.11.023>
- [12] Zhu, R., Zhang, Y., and Yang, D., “Analysis of Mechanical Properties of the Warp Knitted Metal Mesh of Cable-Mesh Antennas,” *Journal of Xidian University*, Vol. 45, No. 2, 2018, pp. 59–65.
- [13] Dušović, M., and Bhattacharya, D., “Simulating the Deformation Mechanisms of Knitted Fabric Composites,” *Compositers Part A: Applied Science and Manufacturing*, Vol. 37, No. 11, 2006, pp. 1897–1915.
<https://doi.org/10.1016/j.compositesa.2005.12.029>
- [14] Sherburn, M., “Geometric and Mechanical Modelling of Textiles.” Ph.D. Dissertation, Univ. of Nottingham, Nottingham, England, U.K., 2007.

R. Ohayon
Associate Editor